Special Issue

n-Butane, *iso*-Butane and 1-Butene Adsorption on Imidazolium-Based Ionic Liquids Studied with Molecular Beam Techniques

Leonhard Winter,[a] Radha G. Bhuin,[a] Florian Maier,[a] and Hans-Peter Steinrück*[a]

Abstract: The interaction of molecules, especially hydrocarbons, at the gas/ionic liquid (IL) surface plays a crucial role in supported IL catalysis. The dynamics of this process is investigated by measuring the trapping probabilities of *n*-butane, *iso*-butane and 1-butene on a set of frozen 1-alkyl-3-methylimidazolium-based ILs $[C_nC_1Im]X$, where $n = 4$, 8 and $X^- = Cl^-$, Br^-, $[PF_6]^-$ and $[Tf_2N]^-$. The decrease of the initial trapping probability with increasing surface temperature is used to determine the desorption energy of the hydrocarbons at the IL surfaces. It increases with increasing alkyl chain length *n* and decreasing anion size for the ILs studied. We attribute these effects to different degrees of alkyl chain surface enrichment, while interactions between the adsorbate and the anion do not play a significant role. The adsorption energy also depends on the adsorbing molecule: It decreases in the order *n*-butane > 1-butene > *iso*-butane, which can be explained by different dispersion interactions.

Introduction

Substances consisting solely of ions and possessing a low melting point, often below room temperature, are classified as ionic liquids (ILs).[1] Although materials fulfilling this definition are known for a long time,[2] extensive research on ILs started only in the 1990s.[3] In the beginning, ILs were seen as "green" alternatives for conventional bulk chemicals,[4] like solvents,[5] electrolytes,[6] lubricants[7] or scavengers.[8] With the years, the "green" label for ILs came increasingly under debate, because of their unknown toxicity,[9] poor biodegradability[10] and cost- and waste-intensive synthesis.[11] In the last years, efforts were made to make ILs environmentally friendlier like using biorenewable raw materials and optimized synthetic routes.[12] An alternative (or additional) strategy to decrease the environmental footprint of ILs is the targeted use of small IL amounts for specific purposes, for example as lubricant additives,[13] pharmaceuticals[14] or in catalysis.[15]

In modern catalytic applications, ILs are often not used as bulk solvents in a biphasic approach, but rather in heterogeneous systems on porous supports.[15d,e] This is realized as Solid Catalysts with Ionic Liquid Layer (SCILL)[16] or Supported Ionic Liquid Phase (SILP) catalysts,[17] which have both found commercial applications.[18] In SCILL, the heterogeneous catalyst is modified by an ionic liquid thin film, which typically improves the catalyst's selectivity.[15d,e,19] In SILP, an originally homogenous catalytic process is "heterogenized" by immobilization of the IL phase containing the dissolved catalyst on an inert porous support, which facilitates product separation and increases the mobile phase/IL interface area.[15d,e,20] In both concepts, the mass transfer across the gas/IL interface plays a crucial role for the selectivity and activity of the catalytic system.

Therefore, the structure of the vacuum/IL interface has been in the center of surface science investigations using different techniques like molecular dynamics calculations,[21] X-ray reflectivity,[22] direct recoil spectrometry,[23] Rutherford backscattering,[23b,24] low energy ion scattering,[25] reactive atom scattering,[26] sum frequency generation vibrational spectroscopy[27] and X-ray photoelectron spectroscopy (XPS).[28] Thereby, a good understanding of the static properties of this interface has been obtained. However, the interaction dynamics of gas molecules at the gas/IL interface has only been investigated for few specific examples: CO_2 is scattered from imidazolium-based ionic liquid surfaces at room temperature by two distinctive pathways, trapping/desorption (TD) and inelastic scattering (IS). The share of the TD pathway increases with increasing alkyl chain length and decreasing anion size.[29] Similar trends were observed for NO scattering, additional to interesting rotational, vibrational and electronic effects occurring for this open-shell molecule.[30] O atoms are scattered inelastically and/or reactively forming OH and H_2O from imidazolium- and pyrrolidinium-based ionic liquids. For both cation classes, the reaction probability increases with increasing alkyl chain length and decreasing anion size.[26a,31] H_2O adsorbs on frozen $[C_2C_1Im][Tf_2N]$ and $[C_8C_1Im][BF_4]$ with an initial trapping probability close to zero, which then increases with coverage. The multilayer (= condensed phase) desorption energy was found to lie above the one of the monolayer (=

[a] L. Winter, Dr. R. G. Bhuin, Dr. F. Maier, Prof. Dr. H.-P. Steinrück
Lehrstuhl für Physikalische Chemie II
Friedrich-Alexander-Universität Erlangen-Nürnberg
Egerlandstr. 3, 91058 Erlangen (Germany)
E-mail: hans-peter.steinrueck@fau.de

Special Issue Part of a Special Issue on Contemporary Challenges in Catalysis.

layer in direct contact with the substrate), which was attributed to strong adsorbate-adsorbate interactions.[32]

Our group has recently reported on the adsorption of *n*-butane from a supersonic molecular beam onto frozen imidazolium-based $[Tf_2N]^-$ and $[PF_6]^-$ ILs.[33] For $[C_1C_1Im]^+$ and $[C_2C_1Im]^+$ cations, no trapping occurs, even at 90 K, which is below the onset of measurable *n*-butane multilayer desorption at 93 K. For cations with at least three carbon atoms in the alkyl side chain, the initial trapping probability is ≈0.9 at 90 K. It decreases with increasing surface temperature, which was attributed to an increasing desorption rate. We developed a procedure to extract the *n*-butane desorption energy from our data, and found that it increases with increasing cation alkyl chain length. In this paper, we aim to extend our work to ILs with the much smaller halides as anions, and to other adsorbates, namely *iso*-butane and 1-butene. The anion dependence of the desorption energy will be rationalized by comparison to the static surface structure probed by angle-resolved X-ray photoelectron spectroscopy (ARXPS).

Experimental Section

The ILs were purchased from IoLiTec Ionic Liquid Technologies GmbH ($[C_8C_1Im][PF_6]$, $[C_4C_1Im][PF_6]$, $[C_4C_1Im]Br$, and $[C_4C_1Im]Cl$, purity >99%) or prepared according to previously published procedures[34] ($[C_8C_1Im][Tf_2N]$, $[C_4C_1Im][Tf_2N]$, and $[C_8C_1Im]Cl$). XPS proved the ILs to be satisfactorily (surface) clean. In particular, we detected none of the IL-typical contaminations, like Si (indicative of silicones) or hydrocarbon species.[35] The quantitative analysis showed that the measured XPS signals agreed with the nominal compositions to within 5%, which is the typical uncertainty of XPS.[34] Only the chloride ILs contained a small oxygen signal indicative of minor amounts of water (4–6 mol%), and a small additional N 1s peak at 400 eV (10% for $[C_8C_1Im]Cl$ and 19% for $[C_4C_1Im]Cl$, possibly due to beam damage). A macroscopic film (≈ 0.5 mm thickness) was spread with a Pasteur pipette on a polycrystalline Ni sample plate ($12\times12\ mm^2$). In the case of the room temperature solids $[C_4C_1Im]Br$ and $[C_4C_1Im]Cl$, the sample plate was gently heated to melt the ILs to ensure homogenous spreading. The samples were introduced via a loadlock into the ultra-high vacuum system (base pressure $\approx 1\cdot10^{-10}$ mbar), which was already described in detail elsewhere.[33b] A type K thermocouple inserted into the sample plate was used to measure the sample temperature, which was controlled by liquid nitrogen cooling and radiation heating with a filament mounted at the back of the sample.

The continuous supersonic molecular beam was generated from a pure *n*-butane, *iso*-butane or 1-butene (purchased from Messer Griesheim, purity >99%) gas stream (1.0 sccm) expanding from a room-temperature nozzle (100 μm diameter). The beam passed a conical skimmer (opening diameter 0.5 mm) and an aperture (1.1 mm diameter) creating a circular beam spot of 3.4 mm diameter. The kinetic energy of the *n*-butane beam was estimated to be approximately 13 kJ/mol by comparison to a similarly generated beam from Ref. [36]. The beam flux was estimated to $2.0\cdot10^{13}\ cm^{-1}\ s^{-1}$.[33a]

The partial pressure in the analysis chamber was measured with a quadrupole mass spectrometer (Hiden Analytical) by recording the time-dependent signal of m/z=43 (*n*-butane and *iso*-butane) or m/z=41 (1-butene), which are the most intense fragments generated from the corresponding molecules by electron ionization (70 eV). A linear background was subtracted from the raw data and an average over the first 0.50 s after opening the sample flag was used to determine the initial trapping probability (see also below). Between two measurements, the IL was heated to 180 K to remove remaining *n*-butane/*iso*-butane/1-butene and other adsorbates potentially contaminating the surface. Water, for example, desorbs from IL surfaces between 140 and 170 K.[32] Heating to higher temperatures was omitted to avoid melting and refreezing of the IL. At least three independently prepared samples were used for each gas/IL combination to ensure reproducibility.

Results and Discussion

The trapping probability *S* represents the probability for an incoming molecule to become trapped, that means adsorbed, on a surface. In our study, we apply the direct method of King and Wells[37] to determine the trapping probability. When applying this method, one uses a supersonic molecular beam with a set of mechanical shutters, also called flags, and measures the background partial pressure. As example, Figure 1 shows typical measurement curves for the adsorption of *n*-butane on two ILs with very different anions, $[C_8C_1Im]Cl$ and $[C_8C_1Im][Tf_2N]$, at ≈90 and 118 K (left side), and a sketch of our setup (right side). The measurement procedure follows a sequence of opening and closing two flags (marked by blue dashed lines in Figure 1), while simultaneously recording the partial pressure of the molecule in the analysis chamber with a quadrupole mass spectrometer (QMS).

In the beginning ($t=-40$ s), the molecular beam is blocked by the beam flag far away from the analysis chamber and the gas is pumped away by differential pumping stages, so that the partial pressure in the analysis chamber is zero. At $t=-20$ s, the beam flag is opened, which allows the molecular beam to enter the analysis chamber, where it is scattered from the inert sample flag. This leads to the pressure increase $\triangle p_{MB}$. At $t=0$ s the sample flag is opened and the molecular beam impinges on the sample surface. If the molecules adsorb on the sample surface, the pressure drops (Figure 1a–c). This initial pressure drop $\triangle p_0$ is used to determine the initial trapping probability S_0 (Equation (1)),

$$S_0 = \frac{\Delta p_0}{\Delta p_{MB}} \tag{1}$$

which corresponds to the trapping probability on the uncovered surface, that is, at zero coverage. If all molecules are scattered from the surface (that is, $S_0=0$), no change in pressure is observed (Figure 1d). Note that in this case in our experiment a small apparent pressure drop occurs, because of an experimental artifact caused by our sample cooling system, for which we apply a correction in our data evaluation procedure.[33b]

If the molecule adsorbs on the surface, a certain coverage builds up, which can influence the trapping probability. A change in the trapping probability will be proportional to a change in partial pressure, so that, analogously to S_0, a time-dependent trapping probability $S(t)$ can be determined from $\triangle p(t)$. In the example of Figure 1c, desorption from the adlayer

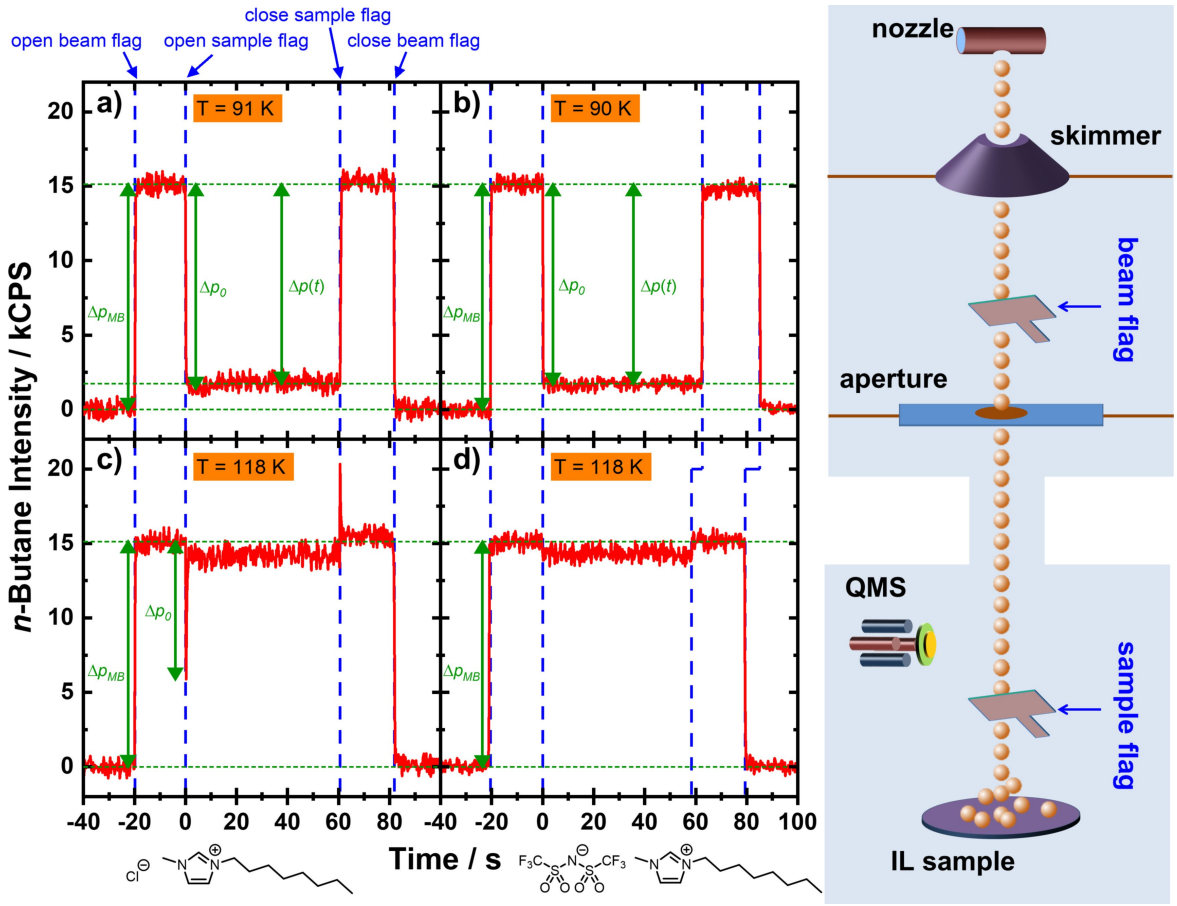

Figure 1. Typical measurement curves obtained with the King and Wells method (left) together with a sketch of the used molecular beam setup (right). The curves show the adsorption dynamics of *n*-butane on $[C_8C_1Im]Cl$ (a, c) and on $[C_8C_1Im][Tf_2N]$ at ≈90/91 and 118 K (b, d). For details see the text.

sets in very quickly, which leads to a very fast pressure increase. After only a few seconds, a steady state situation is reached, in which the adsorption and desorption rates are equal. Thus, the pressure comes back to the level it had before opening the sample flag, so that $S^{net}(t>3\,s)=0$. In cases, where the desorption rate is not zero, the trapping probabilities determined by the King and Wells method are often called "net" trapping probabilities, since they do not represent the probability for an individual molecule to become trapped or scattered, but rather refer to the overall balance between adsorption and desorption rate. In the example of Figures 1a and b, that is, at ≈90 K, the partial pressure remains at a low level, which means that the coverage continues to increase, ultimately leading to multilayer growth.

At $t=60$ s, the sample flag is closed, so that the molecular beam is again scattered by it. The partial pressure returns to the value, which it had during the equivalent situation from −20 to 0 s. In Figure 1c, at 118 K, a spike in the partial pressure curve is visible at $t=60$ s. It is caused by molecules desorbing rapidly from the still present adlayer once the molecular beam does not hit the surface any more. Finally, the beam flag is also closed at $t\approx80$ s and the partial pressure returns to zero.

n-Butane on $[C_nC_1Im]X$ – temperature dependence of S_0^{net}

In the next step, we want to discuss the temperature-dependent behavior of the initial net trapping probability S_0^{net} of *n*-butane on different imidazolium-based ILs. At this point, we will not further address the time-dependence of the trapping probabilities as shown in Figure 1, because the behavior is almost identical for all investigated ILs. Figure 2 shows plots of S_0^{net} vs. T for the set of investigated ILs; part of the results have already been published,[33] but we show them here again, since we are interested in identifying trends upon changing the size of the IL anion. All displayed ILs show a similar S-shaped decrease of S_0^{net} with increasing temperature. For example, for $[C_8C_1Im]Cl$ (black squares in Figure 2a), S_0^{net} stays constant at 0.90 ± 0.05 up to ≈107 K, and thereafter decreases to 0.00 ± 0.05 at $T>126$ K.

At low temperature ($T\leq90$ K), all trapped *n*-butane molecules remain adsorbed on the surface since desorption from the adlayer is negligible. At high temperature ($T\geq127$ K), trapped (that is, thermally accommodated) *n*-butane molecules desorb again almost immediately. We expect that thermal accommodation is very efficient for the unseeded *n*-butane beam generated from our nozzle at room temperature. Firstly, its kinetic energy

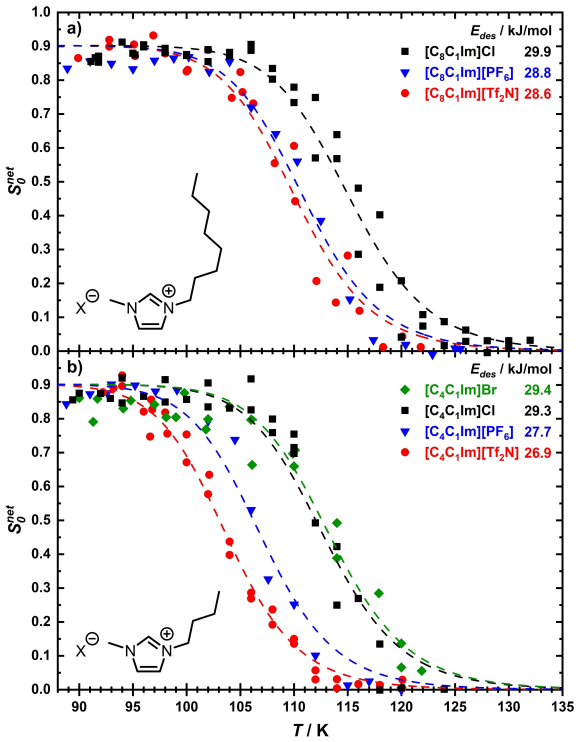

Figure 2. Temperature-dependent initial *n*-butane trapping probabilities of (a) $[C_8C_1Im]X$ (X^-=$[Tf_2N]^-$, $[PF_6]^-$ and Cl^-) and (b) $[C_4C_1Im]X$ (X^-=$[Tf_2N]^-$, $[PF_6]^-$, Cl^- and Br^-). The dashed lines represent fits to the data using Equation (2), in which $S_0^{LT}=0.90$ and $\nu=1.4\cdot10^{14}$ s^{-1} were used as constant parameters for all ILs. Part of the data is already published.[33]

is comparably low (≈13 kJ/mol) and secondly, *n*-butane is a quite heavy and flexible molecule compared to other typical gases like atoms or diatomic molecules. This makes energy transfer from translation to internal rotations and soft vibrations (torsion and bending) very efficient.[38] In the transition region, the residence time of the *n*-butane molecules is in the order of the measurement time required to determine S_0^{net}. We developed a model,[33b] based on the reasonable assumption that thermal accommodation occurs always with the same probability S_0^{LT}, which can be measured at low temperature, where desorption is negligible. S_0^{net} is then given by Equation (2)

$$S_0^{net} = \frac{S_0^{LT}}{1 + \frac{t_m}{2}\cdot\nu\cdot e^{-\frac{E_{des}}{RT}}} \qquad (2)$$

where t_m is the measurement time (in our case 0.50 s), ν the pre-exponential factor, R the universal gas constant and E_{des} the desorption energy, which in case of non-activated adsorption is equal to the adsorption or binding energy. Figure 2 shows the results of fitting Equation (2) to the data as dashed lines. Note that S_0^{net} is indeed influenced by the chosen t_m, but E_{des} does not change if a different t_m is used for evaluation. Since ν and E_{des} are strongly coupled, it is necessary to constrain one of them to obtain unambiguous fitting results. In our evaluation, we used $\nu=1.4\cdot10^{14}$ s^{-1}; this value was found in an Arrhenius-type analysis of time-dependent *n*-butane trapping probabilities on $[C_8C_1Im][Tf_2N]$.[33a] Since the adsorbate remains the same and the binding motif is expected to be similar, that is, the interaction is dominated by the IL alkyl chains, we assume that this pre-exponential factor holds for all ILs. Overall, the relative accuracy of our approach is estimated to ±0.3 kJ/mol. Relative accuracy refers hereby to comparing data measured with the same experimental setup, which is the case here. However, the absolute accuracy is estimated to ±2 kJ/mol, which is due to the uncertainty of the pre-exponential factor and the absolute thermocouple reading at these low temperatures (±3 K).

n-Butane on $[C_nC_1Im]X$ – trends in the desorption energy

The data for the imidazolium-based ILs with different lengths of the alkyl chain ($n=4$ and 8) and different anions (Cl^-, Br^-, $[PF_6]^-$ and $[Tf_2N]^-$) in Figure 2 shows two trends: Firstly, E_{des} increases with increasing alkyl chain length, so that the curves in Figure 2a for the $[C_8C_1Im]X$ series are shifted to higher temperature compared to the corresponding curves in Figure 2b for the $[C_4C_1Im]X$ series. Secondly, E_{des} increases with decreasing size of the anion, that is, in the order $[Tf_2N]^- < [PF_6]^- < Br^- \approx Cl^-$. For example, in the $[C_4C_1Im]X$ series E_{des} increases from 26.9 kJ/mol ($[Tf_2N]^-$) via 27.7 kJ/mol ($[PF_6]^-$) to 29.3 kJ/mol (Cl^-) and 29.4 kJ/mol (Br^-).

A readily available quantitative measure for the anion size is the molecular volume, which can be easily calculated from literature density data (obtained from the NIST ILThermo database[39]). Figure 3a shows the correlation of E_{des} with the molecular volume for the two investigated groups of ILs, $[C_8C_1Im]X$ as open symbols and $[C_4C_1Im]X$ as filled symbols. Apparently, the correlation is not linear, but a rather steep decrease of E_{des} is found from the halide anions to $[PF_6]^-$, followed by a more shallow decrease from $[PF_6]^-$ to $[Tf_2N]^-$.

While Figure 3a indicates a correlation between the observed initial adsorption behavior and the bulk molecular volume of the ILs, one rather expects a dependence on surface properties. Indeed, it has been demonstrated that the outer surface layer of ILs considerably differs from the average bulk composition. In particular, the size of the anion has a strong impact on the degree of surface enrichment of the imidazolium alkyl chains protruding into the vacuum. This behavior has been demonstrated by a number of theoretical studies and experimental investigations including molecular dynamics simulations,[21b,40] reactive atom scattering,[26a,31a] Rutherford backscattering[23b,41] and X-ray photoelectron spectroscopy.[34,42] Especially the last method provides a very convenient way to quantify the degree of alkyl chain enrichment: Imidazolium-based cations show two peaks in the C 1s region, one belonging to the carbon atoms bound to at least one nitrogen atom (called C_{hetero}) and one belonging to the carbon atoms bound only to carbon and hydrogen (called C_{alkyl}). The ratio of the peak areas $I_{C\,1s}(C_{alkyl})/I_{C\,1s}(C_{hetero})$ is expected to be 7:5=1.4 for $[C_8C_1Im]X$ and 3:5=0.6 for $[C_4C_1Im]X$ based on the stoichiometries of the ILs (see dotted horizontal lines in Figure 3b). These ratios were indeed found for XPS measure-

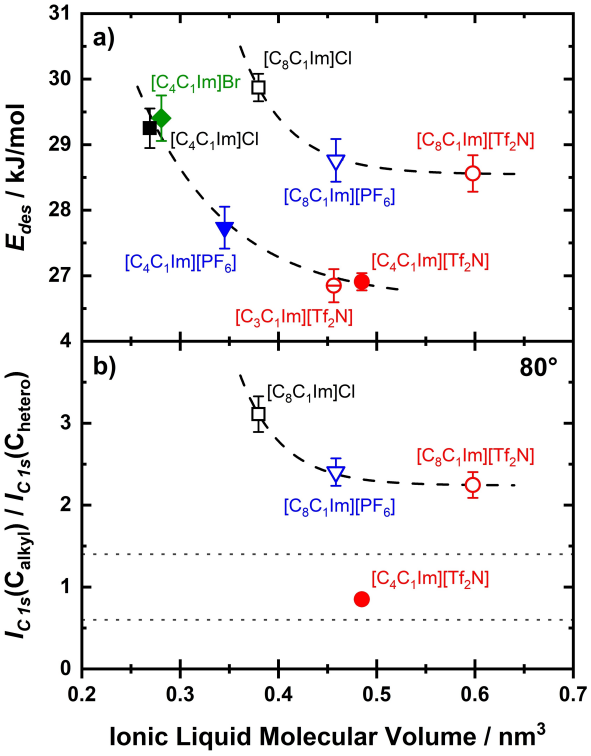

Figure 3. Comparison of (a) *n*-butane desorption energy and (b) alkyl chain surface enrichment. The datasets are plotted vs. the IL's molecular volume to visualize the effect of the anion size. Color codes and open/filled symbols are used to group the ILs by their anion and cation identity. The dashed lines serve as a guide for the eye. The molecular volumes were calculated from the IL densities at 298.15 K, 101.325 kPa, for which an average over the values published in the ILThermo database from NIST[39] were used. Some of the values for E_{des} are already published.[33b] The error bars indicate the estimated uncertainty, by assuming an identical prefactor for all ILs (for details see text). The data from (b) were adapted from previously published studies of our group.[34,42b] The dotted lines in (b) indicate the nominal C_{alkyl}/C_{hetero} ratios for $[C_8C_1Im]^+$ (=1.4) and $[C_4C_1Im]^+$ (=0.6).

ments in 0° emission angle (information depth ≈8.4 nm), but for measurements at a surface-sensitive emission angle of 80° (information depth ≈1.5 nm) ratios higher than the nominally expected ones were obtained.[34,42b,c] Comparing the peak ratios at 80° emission of different ILs showed that the degree of enrichment increases with increasing chain length[34] and with decreasing anion size.[42b] The latter can be explained by a denser packing of the imidazolium cations if they are incorporated into an ionic sublayer with smaller anions, which in turn also leads to a denser packing of the protruding alkyl chains. A selection of this literature data is shown in Figure 3b, where the C_{alkyl}/C_{herero} ratio is plotted for several ILs.

The two datasets compiled in Figure 3 demonstrate that the alkyl enrichment derived by XPS and the *n*-butane desorption energies derived by the King and Wells method show the same trends with increasing molecular volume. For both, a steep decrease from Cl^- (black symbols) to $[PF_6]^-$ (blue) is followed by a shallow further decrease to $[Tf_2N]^-$ (red). Furthermore, the values strongly increase from $[C_4C_1Im]^+$ (full symbols) to $[C_8C_1Im]^+$ (open symbols). Thus, we conclude that the interaction strength of *n*-butane with the IL surface critically depends on the alkyl chain enrichment. The interaction of *n*-butane with the alkyl chains is stronger than with the imidazolium headgroups and the anions, as is proven by the fact that *n*-butane does not adsorb on ILs with the $[C_2C_1Im]^+$ cation, which only possesses a very short alkyl chain.[33a] The changes in the desorption energy observed for different anions are not caused by interactions between *n*-butane and the anion, but by the different IL surface structure induced by the anion.

iso-Butane and 1-butene on $[C_8C_1Im][Tf_2N]$

So far, we used *n*-butane as a model system to study the adsorption of hydrocarbons on different IL surfaces. Since the adsorption dynamics, however, will also be influenced by the nature of the hydrocarbon, we studied the adsorption of two other C4 hydrocarbons on $[C_8C_1Im][Tf_2N]$, and compare the observed behavior with the already published results for *n*-butane.[33] *iso*-Butane is the isomer of *n*-butane and 1-butene is an unsaturated analogue of *n*-butane. The molecular structures and the temperature-dependent initial trapping probabilities are shown in Figure 4. At low temperature ($T \approx 90$ K), all three hydrocarbons show the same trapping probability $S_0^{LT} = 0.90 \pm 0.05$. This shows that thermal accommodation is equally efficient for all three hydrocarbons at our experimental conditions, although the different molecular structures could principally result in different energy transfer mechanisms to bending and torsion modes.

For *iso*-butane and 1-butene, S_0^{net} shows a similar S-shaped decrease, as it was found for *n*-butane. This allows us to determine the desorption energy by fitting Equation (2) to the data, assuming the same pre-exponential factor $\nu = 1.4 \cdot 10^{14}$ s^{-1} for all three hydrocarbons. We observe that the desorption energy decreases from 28.6 kJ/mol (*n*-butane) via 27.9 kJ/mol (1-butene) to 27.5 kJ/mol (*iso*-butane). Interestingly, this trend is

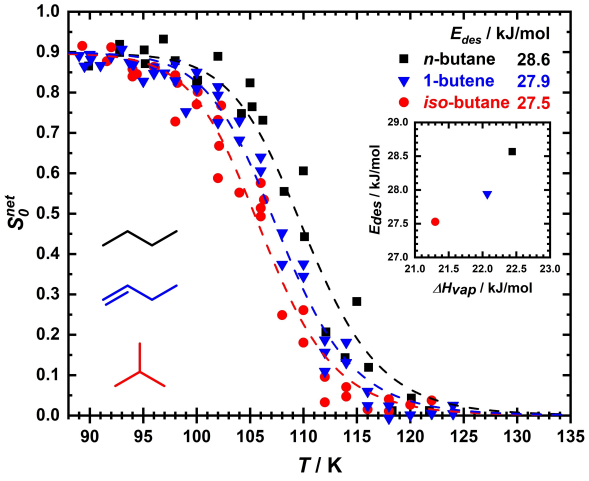

Figure 4. Temperature-dependent initial trapping probabilities of *iso*-butane, 1-butene and *n*-butane on $[C_8C_1Im][Tf_2N]$. The dashed lines represent fits to the datasets according to Equation (2). The inset shows the correlation between E_{des} and the enthalpies of vaporization.[43]

correlated with the enthalpies of vaporization[43] of the pure hydrocarbons, as is evident from the inset in Figure 4. The differences in the enthalpies of vaporization for the three compounds are caused by the dispersion forces between one molecule and its neighbors of the same kind. These forces decrease in the order *n*-butane > 1-butene > *iso*-butane, which is mainly caused by better intermolecular alignment of elongated compared to ball-like molecules. The situation at the IL surface is somewhat similar: Since the molecule/IL interaction is dominated by the interaction with the IL alkyl chains (on ILs with short chains no adsorption occurs), the hydrocarbon molecules will align with the IL alkyl chains, so that also in this case the interaction is the strongest for *n*-butane and the weakest for *iso*-butane with 1-butene lying somewhere in between.

Conclusion

We determined the trapping probabilities for *n*-butane on a series of imidazolium-based $[C_nC_1Im]X$ ($n = 4$, 8; $X^- = Cl^-$, Br^-, $[PF_6]^-$, $[Tf_2N]^-$) ionic liquids by the direct method of King and Wells.[37] Furthermore, we compared the behavior for *n*-butane with that of *iso*-butane and 1-butene on $[C_8C_1Im][Tf_2N]$. *n*-Butane adsorbs at 90 K with an initial trapping probability of 0.90 ± 0.05 on all ILs investigated. With increasing surface temperature, the trapping probability decreases to zero forming an S-shaped curve. This characteristic decrease shifts to higher temperatures for longer alkyl chains and smaller anions, which can be attributed to an increase in desorption energy. The pronounced dependence on the alkyl chain length indicates that *n*-butane mainly interacts with the alkyl chains and the interaction with the anion and the cationic headgroup is only weak.[33a] The desorption energy also increases with decreasing anion size: While only a weak increase is seen from $[Tf_2N]^-$ to $[PF_6]^-$, a quite strong increase occurs when going to Cl^- and Br^-. The exact same trend was observed previously in X-ray photoelectron spectroscopy measurements of the alkyl chain enrichment.[42b] Therefore, we conclude that the observed differences are not due to *n*-butane adsorption on the anion moiety, but rather by an increasingly denser packing of the alkyl chains when decreasing the size of the anion.

iso-Butane and 1-butene also show an initial trapping probability of 0.90 ± 0.05 at 90 K and an S-shaped decrease with increasing surface temperature. This decrease is shifted to lower temperatures in the order *n*-butane > 1-butene > *iso*-butane, again attributed to a decrease in desorption energy in the same order. This finding can be explained by the intermolecular dispersion forces between the gas molecule and the IL surface, which are expected to be strongest for *n*-butane and weakest for *iso*-butane.

Our study shows that the interactions of molecules with IL surfaces are dominated by the specific groups (here alkyl chains) at the outermost surface as well as by the properties of the molecules. This knowledge is a first step for the rational design of gas/IL interfaces, which are of high relevance for the SILP and SCILL concepts, for both of which the interaction of the reactants with the IL surface is the first and possibly decisive step for their functionality. Another possible application is separation technology. For the here studied molecules, the differences in adsorption strength are quite small, however, so that a successful application in this area does not seem feasible to us. Further studies with different ILs and different molecules are required to obtain a more general picture.

Acknowledgements

L.W., R.G.B. and H.-P.S. thank the European Research Council (ERC) under the European Union's Horizon 2020 research and innovation programme for financial support, in the context of the Advanced Investigator Grant "ILID" to H.-P.S. (Grant Agreement No. 693398-ILID). We thank Dr. Matthias Lexow for fruitful discussions. Open Access funding enabled and organized by Projekt DEAL.

Conflict of Interest

The authors declare no conflict of interest.

Keywords: adsorption · catalysis · gas-surface dynamics · ionic liquids · molecular beam

[1] a) P. Wasserscheid, T. Welton, *Ionic liquids in synthesis*, Wiley-VCH, Weinheim **2003**; b) D. R. MacFarlane, M. Kar, J. M. Pringle, *Fundamentals of Ionic Liquids*, Wiley-VCH, Weinheim **2017**.
[2] P. Walden, *Bull. Acad. Imp. Sci. St.-Petersbourg* **1914**, 405–422.
[3] a) J. S. Wilkes, M. J. Zaworotko, *J. Chem. Soc. Chem. Commun.* **1992**, 965–967; b) T. Welton, *Biophys. Rev. Lett.* **2018**, *10*, 691–706.
[4] a) K. R. Seddon, *J. Chem. Technol. Biotechnol.* **1997**, *68*, 351–356; b) J. G. Huddleston, H. D. Willauer, R. P. Swatloski, A. E. Visser, R. D. Rogers, *Chem. Commun.* **1998**, 1765–1766; c) M. J. Earle, K. R. Seddon, *Pure Appl. Chem.* **2000**, *72*, 1391–1398.
[5] a) T. Welton, *Chem. Rev.* **1999**, *99*, 2071–2084; b) R. D. Rogers, K. R. Seddon, *Science* **2003**, *302*, 792–793; c) J. P. Hallett, T. Welton, *Chem. Rev.* **2011**, *111*, 3508–3576.
[6] a) M. Galiński, A. Lewandowski, I. Stępniak, *Electrochim. Acta* **2006**, *51*, 5567–5580; b) P. Hapiot, C. Lagrost, *Chem. Rev.* **2008**, *108*, 2238–2264; c) M. Watanabe, M. L. Thomas, S. Zhang, K. Ueno, T. Yasuda, K. Dokko, *Chem. Rev.* **2017**, *117*, 7190–7239; d) M. Forsyth, L. Porcarelli, X. Wang, N. Goujon, D. Mecerreyes, *Acc. Chem. Res.* **2019**, *52*, 686–694.
[7] a) I. Minami, *Molecules* **2009**, *14*, 2286–2305; b) M. Cai, Q. Yu, W. Liu, F. Zhou, *Chem. Soc. Rev.* **2020**, *49*, 7753–7818.
[8] a) M. Maase, K. Massonne, *Ionic Liquids IIIB: Fundamentals, Progress, Challenges, and Opportunities: Transformations and Processes*, Vol. 902 (Eds.: R. D. Rogers, K. R. Seddon), American Chemical Society **2005**, pp. 126–132; b) M. Ramdin, T. W. de Loos, T. J. H. Vlugt, *Ind. Eng. Chem. Res.* **2012**, *51*, 8149–8177; c) S. Zeng, X. Zhang, L. Bai, X. Zhang, H. Wang, J. Wang, D. Bao, M. Li, X. Liu, S. Zhang, *Chem. Rev.* **2017**, *117*, 9625–9673.
[9] R. F. M. Frade, C. A. M. Afonso, *Hum. Exp. Toxicol.* **2010**, *29*, 1038–1054.
[10] S. P. F. Costa, A. M. O. Azevedo, P. C. A. G. Pinto, M. L. M. F. S. Saraiva, *ChemSusChem* **2017**, *10*, 2321–2347.
[11] a) J. H. Clark, S. J. Tavener, *Org. Process Res. Dev.* **2007**, *11*, 149–155; b) P. G. Jessop, *Green Chem.* **2011**, *13*, 1391–1398; c) G. Cevasco, C. Chiappe, *Green Chem.* **2014**, *16*, 2375–2385.
[12] a) B. L. Gadilohar, G. S. Shankarling, *J. Mol. Liq.* **2017**, *227*, 234–261; b) J. M. Gomes, S. S. Silva, R. L. Reis, *Chem. Soc. Rev.* **2019**, *48*, 4317–4335; c) B. Gaida, A. Brzęczek-Szafran, *Molecules* **2020**, *25*, 3285.
[13] Y. Zhou, J. Qu, *ACS Appl. Mater. Interfaces* **2017**, *9*, 3209–3222.

[14] a) I. M. Marrucho, L. C. Branco, L. P. N. Rebelo, *Annu. Rev. Chem. Biomol. Eng.* **2014**, *5*, 527–546; b) K. S. Egorova, E. G. Gordeev, V. P. Ananikov, *Chem. Rev.* **2017**, *117*, 7132–7189.
[15] a) Y. Qiao, W. Ma, N. Theyssen, C. Chen, Z. Hou, *Chem. Rev.* **2017**, *117*, 6881–6928; b) C. Dai, J. Zhang, C. Huang, Z. Lei, *Chem. Rev.* **2017**, *117*, 6929–6983; c) B. Karimi, M. Tavakolian, M. Akbari, F. Mansouri, *ChemCatChem* **2018**, *10*, 3173–3205; d) H.-P. Steinrück, P. Wasserscheid, *Catal. Lett.* **2015**, *145*, 380–397; e) O. Bartlewicz, I. Dąbek, A. Szymańska, H. Maciejewski, *Catalysts* **2020**, *10*, 1227.
[16] U. Kernchen, B. Etzold, W. Korth, A. Jess, *Chem. Eng. Technol.* **2007**, *30*, 985–994.
[17] C. P. Mehnert, R. A. Cook, N. C. Dispenziere, M. Afeworki, *J. Am. Chem. Soc.* **2002**, *124*, 12932–12933.
[18] A. J. Greer, J. Jacquemin, C. Hardacre, *Molecules* **2020**, *25*, 5207.
[19] W. Korth, A. Jess, *Supported Ionic Liquids*, (Eds.: R. Fehrmann, A. Riisager, M. Haumann), Wiley-VCH, Weinheim **2014**, pp. 279–306.
[20] a) A. Schönweiz, R. Franke, *Supported Ionic Liquids* (Eds.: R. Fehrmann, A. Riisager, M. Haumann), Wiley-VCH, Weinheim **2014**, pp. 307–326; b) J. M. Marinkovic, A. Riisager, R. Franke, P. Wasserscheid, M. Haumann, *Ind. Eng. Chem. Res.* **2019**, *58*, 2409–2420.
[21] a) R. M. Lynden-Bell, *Mol. Phys.* **2003**, *101*, 2625–2633; b) K. Shimizu, B. S. J. Heller, F. Maier, H.-P. Steinrück, J. N. Canongia Lopes, *Langmuir* **2018**, *34*, 4408–4416.
[22] a) A. J. Carmichael, C. Hardacre, J. D. Holbrey, K. R. Seddon, M. Nieuwenhuyzen, *Proc. Vol. 1999* **1999**, *41*, 209–221; b) J. Haddad, D. Pontoni, B. M. Murphy, S. Festersen, B. Runge, O. M. Magnussen, H.-G. Steinrück, H. Reichert, B. M. Ocko, M. Deutsch, *Proc. Natl. Acad. Sci. USA* **2018**, *115*, E1100–E1107.
[23] a) T. J. Gannon, G. Law, P. R. Watson, A. J. Carmichael, K. R. Seddon, *Langmuir* **1999**, *15*, 8429–8434; b) K. Nakajima, M. Lísal, K. Kimura, *Surface and Interface Science*, Vol. 7 (Ed.: K. Wandelt), Wiley-VCH, Weinheim **2020**, pp. 351–389.
[24] K. Nakajima, A. Ohno, M. Suzuki, K. Kimura, *Langmuir* **2008**, *24*, 4482–4484.
[25] a) S. Caporali, U. Bardi, A. Lavacchi, *J. Electron Spectrosc.* **2006**, *151*, 4–8; b) I. J. Villar-Garcia, S. Fearn, G. F. De Gregorio, N. L. Ismail, F. J. V. Gschwend, A. J. S. McIntosh, K. R. J. Lovelock, *Chem. Sci.* **2014**, *5*, 4404–4418.
[26] a) B. Wu, J. Zhang, T. K. Minton, K. G. McKendrick, J. M. Slattery, S. Yockel, G. C. Schatz, *J. Phys. Chem. C* **2010**, *114*, 4015–4027; b) E. J. Smoll, S. M. Purcell, L. D'Andrea, J. M. Slattery, D. W. Bruce, M. L. Costen, K. G. McKendrick, T. K. Minton, *J. Phys. Chem. Lett.* **2019**, *10*, 156–163.
[27] a) S. Baldelli, *J. Phys. Chem. B* **2003**, *107*, 6148–6152; b) T. Iwahashi, T. Ishiyama, Y. Sakai, A. Morita, D. Kim, Y. Ouchi, *Phys. Chem. Chem. Phys.* **2020**, *22*, 12565–12576.
[28] a) E. F. Smith, F. J. M. Rutten, I. J. Villar-Garcia, D. Briggs, P. Licence, *Langmuir* **2006**, *22*, 9386–9392; b) K. R. J. Lovelock, I. J. Villar-Garcia, F. Maier, H.-P. Steinrück, P. Licence, *Chem. Rev.* **2010**, *110*, 5158–5190; c) H.-P. Steinrück, *Phys. Chem. Chem. Phys.* **2012**, *14*, 5010–5029; d) C. Kolbeck, I. Niedermaier, A. Deyko, K. R. J. Lovelock, N. Taccardi, W. Wei, P. Wasserscheid, F. Maier, H.-P. Steinrück, *Chem. Eur. J.* **2014**, *20*, 3954–3965; e) S. Men, D. S. Mitchell, K. R. J. Lovelock, P. Licence, *ChemPhysChem* **2015**, *16*, 2211–2218; f) B. S. J. Heller, M. Lexow, F. Greco, S. Shin, G. Partl, F. Maier, H.-P. Steinrück, *Chem. Eur. J.* **2020**, *26*, 1117–1126.
[29] a) J. R. Roscioli, D. J. Nesbitt, *J. Phys. Chem. Lett.* **2010**, *1*, 674–678; b) J. R. Roscioli, D. J. Nesbitt, *J. Phys. Chem. A* **2011**, *115*, 9764–9773.
[30] a) M. P. Ziemkiewicz, A. Zutz, D. J. Nesbitt, *J. Phys. Chem. C* **2012**, *116*, 14284–14294; b) A. Zutz, D. J. Nesbitt, *AIP Adv.* **2016**, *6*, 105207.
[31] a) M. A. Tesa-Serrate, B. C. Marshall, E. J. Smoll, S. M. Purcell, M. L. Costen, J. M. Slattery, T. K. Minton, K. G. McKendrick, *J. Phys. Chem. C* **2015**, *119*, 5491–5505; b) B. C. Marshall, E. J. Smoll, S. M. Purcell, M. L. Costen, K. G. McKendrick, T. K. Minton, *J. Phys. Chem. C* **2016**, *120*, 12472–12483; c) M. A. Tesa-Serrate, E. J. Smoll, L. D'Andrea, S. M. Purcell, M. L. Costen, D. W. Bruce, J. M. Slattery, T. K. Minton, K. G. McKendrick, *J. Phys. Chem. C* **2016**, *120*, 27369–27379.
[32] A. Deyko, R. G. Jones, *Faraday Discuss.* **2012**, *154*, 265–288.
[33] a) R. G. Bhuin, L. Winter, M. Lexow, F. Maier, H.-P. Steinrück, *Angew. Chem. Int. Ed.* **2020**, *59*, 14429–14433; *Angew. Chem.* **2020**, *132*, 14536–14541; b) L. Winter, R. G. Bhuin, M. Lexow, F. Maier, H.-P. Steinrück, *J. Chem. Phys.* **2020**, *153*, 214706.
[34] K. R. J. Lovelock, C. Kolbeck, T. Cremer, N. Paape, P. S. Schulz, P. Wasserscheid, F. Maier, H.-P. Steinrück, *J. Phys. Chem. B* **2009**, *113*, 2854–2864.
[35] J. M. Gottfried, F. Maier, J. Rossa, D. Gerhard, P. S. Schulz, P. Wasserscheid, H.-P. Steinrück, *Z. Phys. Chem.* **2006**, *220*, 1439–1453.
[36] A. V. Hamza, H.-P. Steinrück, R. J. Madix, *J. Chem. Phys.* **1986**, *85*, 7494–7495.
[37] D. A. King, M. G. Wells, *Surf. Sci.* **1972**, *29*, 454–482.
[38] J. F. Weaver, A. F. Carlsson, R. J. Madix, *Surf. Sci. Rep.* **2003**, *50*, 107–199.
[39] Q. Dong, C. D. Muzny, A. Kazakov, V. Diky, J. W. Magee, J. A. Widegren, R. D. Chirico, K. N. Marsh, M. Frenkel, *J. Chem. Eng. Data* **2007**, *52*, 1151–1159.
[40] R. M. Lynden-Bell, M. Del Pópolo, *Phys. Chem. Chem. Phys.* **2006**, *8*, 949–954.
[41] A. Ohno, H. Hashimoto, K. Nakajima, M. Suzuki, K. Kimura, *J. Chem. Phys.* **2009**, *130*, 204705.
[42] a) V. Lockett, R. Sedev, C. Bassell, J. Ralston, *Phys. Chem. Chem. Phys.* **2008**, *10*, 1330–1335; b) C. Kolbeck, T. Cremer, K. R. J. Lovelock, N. Paape, P. S. Schulz, P. Wasserscheid, F. Maier, H.-P. Steinrück, *J. Phys. Chem. B* **2009**, *113*, 8682–8688; c) F. Maier, T. Cremer, C. Kolbeck, K. R. J. Lovelock, N. Paape, P. S. Schulz, P. Wasserscheid, H.-P. Steinrück, *Phys. Chem. Chem. Phys.* **2010**, *12*, 1905–1915; d) S. Men, B. B. Hurisso, K. R. J. Lovelock, P. Licence, *Phys. Chem. Chem. Phys.* **2012**, *14*, 5229–5238.
[43] V. Majer, V. Svoboda, *Enthalpies of Vaporization of Organic Compounds: A Critical Review and Data Compilation*, Blackwell Scientific Publications, Oxford **1985**.

Manuscript received: July 9, 2021
Accepted manuscript online: September 9, 2021
Version of record online: September 29, 2021

